

NANTEN ^{12}CO ($J=1 \rightarrow 0$) observations around the star WR 55

N. U. Duronea¹, E. M. Arnal^{1,2}, and J. C. Testori¹

¹ Instituto Argentino de Radioastronomía, CONICET, CCT-La Plata, C.C.5., 1894 Villa Elisa, Argentina
e-mail: duronea@iar.unlp.edu.ar

² Facultad de Ciencias Astronómicas y Geofísicas, Universidad Nacional de La Plata, Paseo del Bosque s/n, 1900 La Plata, Argentina

Received 30 December 2011 / Accepted 7 February 2012

ABSTRACT

Context. We present a complete study of the molecular and ionized gas in the environs of the nebula RCW 78 around WR 55.

Aims. We investigate the spatial distribution, physical characteristics, and kinematical properties of the molecular gas linked to the galactic nebula RCW 78 to obtain a clearer understanding of its interaction with both the star and the ionized gas.

Methods. Our study is based on $^{12}\text{CO}(1-0)$ fully sampled observations of a region of $\sim 0.45'$ in size around the star WR 55 and the nebula RCW 78 obtained with the 4-m NANTEN telescope, radio continuum archival data at 1.4 and 4.85 GHz, obtained from the SGPS and PMNRAO Southern Radio Survey, respectively, and available infrared MIPS GAL images at $24\ \mu\text{m}$.

Results. A molecular gas component in the velocity range from $\sim -58\ \text{km s}^{-1}$ to $-45\ \text{km s}^{-1}$, which is compatible with the velocity of the ionized gas, was found to be associated with the optical nebula. Adopting a distance of $\sim 5\ \text{kpc}$, the mass of this molecular component is about $3.4 \times 10^4\ M_\odot$. Our analysis of the molecular data reveals a velocity gradient that is consistent with that found for the $\text{H}\alpha$ line. New radio-continuum flux-density determinations confirm the thermal nature of RCW 78. This indicates that the ionized gas in RCW 78 arises from the photoionization of the molecular gas component in the velocity range from $-58\ \text{km s}^{-1}$ to $-45\ \text{km s}^{-1}$. A molecular concentration at a velocity of $-56.1\ \text{km s}^{-1}$ (identified as C1) is likely associated with the star HD 117797 and with an ensemble of candidate YSOs, lying at a distance of $3.9\ \text{kpc}$, while the rest of the molecular gas at velocities between $-56\ \text{km s}^{-1}$ and $-46\ \text{km s}^{-1}$ constitute an incomplete ring-like structure expanding around WR 55 at a velocity of about $\sim 5\ \text{km s}^{-1}$. Mechanical energy and time requirements indicate that WR 55 is very capable of sustaining the expansion of the nebula.

Key words. ISM: molecules – stars: Wolf-Rayet – HII regions

1. Introduction

Wolf-Rayet (WR) stars are the descendants of massive ($\geq 25\ M_\odot$) O-type stars and represent the last evolutionary phase of a massive stellar object prior to its explosion as a supernova. The WR stars are some of the most powerful sources of ionizing radiation and have lost a significant portion of their atmospheres through intense winds, leading to the formation of the well-known “WR ring nebulae” (WRRN) (Chu 1981) and/or “interstellar bubbles” (IB) (Castor et al. 1975; Dyson 1977; Weaver et al. 1977). Both WRRN and IBs are consistent with the typical evolution of an O-type star to the WR phase through a sequence of three stages. In the course of this evolutionary path, each stage is characterized by a different kind of wind (Garcia-Segura & Mac Low 1995). During the O phase, the gas around the star is first ionized by the high Lyman continuum flux, producing an HII region that expands in the surrounding cold neutral medium as a result of its higher pressure. Afterwards, the HII region is evacuated via powerful stellar winds creating an IB, examples of which have been successfully detected mainly in the 21 cm line of atomic hydrogen (Arnal 1992; Arnal & Cappa 1996; Cappa et al. 1996; Arnal et al. 1999; Vasquez et al. 2005). When the star becomes a red supergiant (RSG), the stellar wind is dense and has a low terminal velocity. Afterwards, the WR phase begins, and their fast wind rapidly reaches and interacts with the previous RSG wind creating a WRRN.

The physics and kinematics of molecular gas around ring nebulae and IBs are far from being completely understood. During the expansion of the HII region, a dense shell of neutral material accumulates between the ionization front (IF) and the

shock front (SF), which in an ideal case completely surrounds either the HII region or the IB. In most of the cases studied so far, the molecular gas is interstellar in origin, and shows signs of interaction with the stellar radiation and winds (Rizzo et al. 2001a,b; Cappa et al. 2001; Marston 2001; Vasquez et al. 2009).

RCW 78 is a WRRN that was first discovered in the catalogue of H α emission regions of the Southern Milky Way produced by Rodgers et al. (1960). The brightest part of this nebula is about $15'$ in diameter and is centered on the position of the star HD 117688 (Fig. 1). HD 117688 (\equiv WR 55) is a WN7 star located at $(l, b) = (307^\circ 80, +0^\circ 160)$ (van der Hucht 2001) and the H α ring nebula RCW 78 is likely to be associated with this star. About $7'$ southeast of WR 55 (in equatorial coordinates) the open cluster C1331-622 is located. This cluster is $\sim 7'$ in diameter and $820\ \text{pc}$ (Dias et al. 2010) away from the Sun. The O8Ib(f) star (Walborn 1982) HD 117797, which is located at $(l, b) = (307^\circ 8593, +0^\circ 0447)$, is seen projected onto C1331-622. This star is located at a distance of $3.9 \pm 1.0\ \text{kpc}$ (Turner & Forbes 2005) and is unlikely to be related to the open cluster C1331-622. The error in the distance of HD 117797 stems from assuming a cosmic dispersion of 0.5 in absolute magnitude (Walborn 1972). The location of HD 117797 prevents us from determining whether the intense H α emission observed towards lower Galactic longitudes is caused by nebular emission associated with this star or is part of RCW 78. The IRAS source 13316-6210 is situated almost $\sim 5'$ eastwards of HD 117797.

The distance of WR 55 and its associated nebula is far from being known. On the one hand, several authors quote distances in the range from $4.0\ \text{kpc}$ to $5.0\ \text{kpc}$ (Georgelin et al. 1988; Cappa et al. 2009), while others authors have determined distances

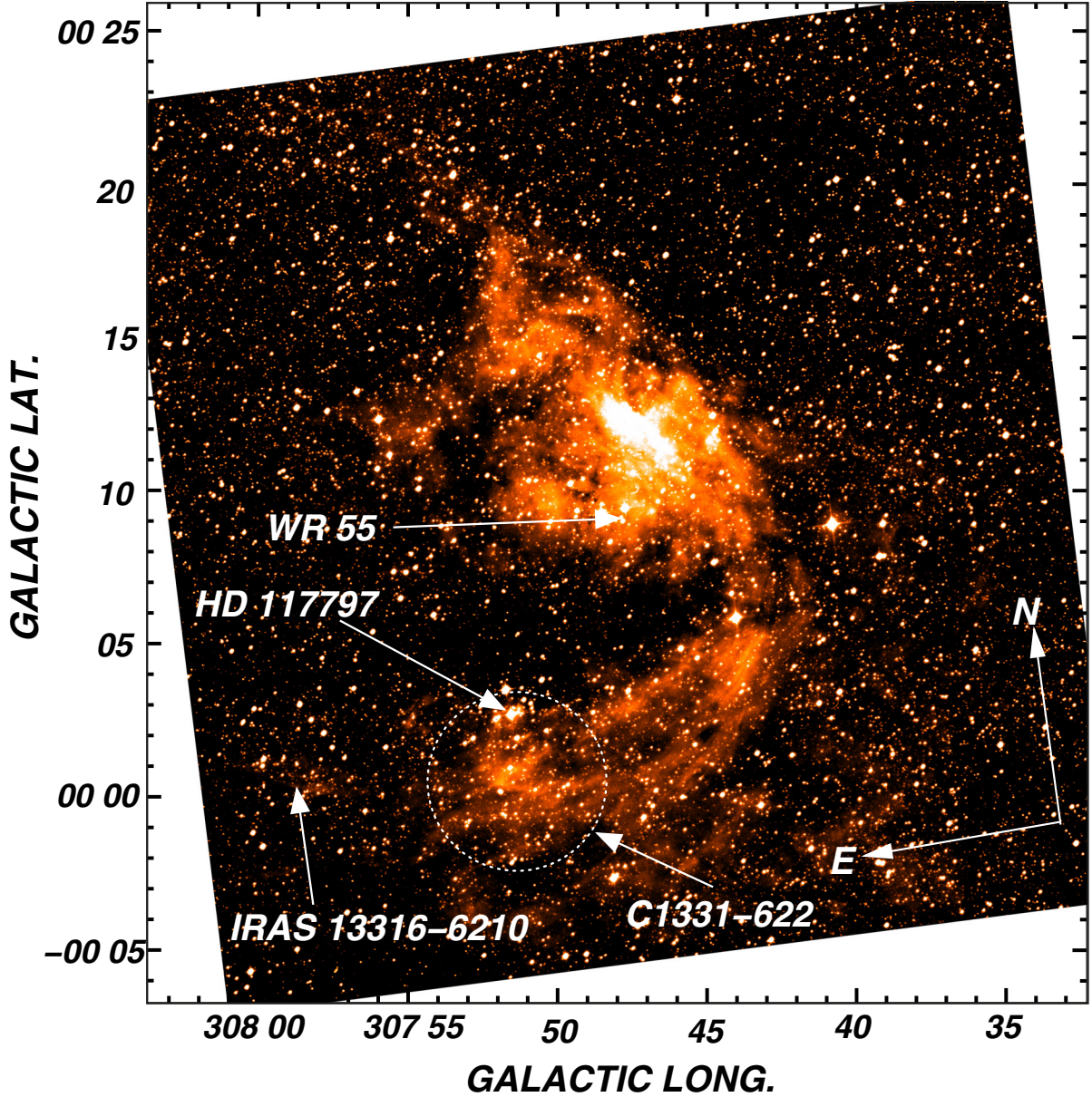


Fig. 1. SuperCOSMOS H α image of the brightest part of the ring nebula RCW 78. The position of different objects in the field are indicated (see text). The orientation of the equatorial system is given by the arrows labeled E (east) and N (north).

mostly in the range from 5.5 kpc to 7.6 kpc (Chu & Treffers 1981; Conti & Vacca 1990; van der Hucht 2001).

Several spectroscopic studies of RCW 78 have been carried out in the past. Chu & Treffers (1981) showed that the H α line at the brightest central part of the nebula displays a slight north-south velocity gradient. The velocity of the H α line varies from -44 km s^{-1} (at the position of WR 55) to -53.4 km s^{-1} ($\sim 7'$ northwards of WR 55). These authors claimed that this gradient is the result of an outflow of the ionized gas at the surface of a molecular cloud. They classified RCW 78 as R $_{\alpha}$ -type nebula (amorphous) since no signs of expansion were found. Spatially resolved spectroscopy was carried out by Esteban et al. (1990). The derived abundances of nitrogen and helium are consistent with self-enrichment. Esteban (1993) later claimed that photoionization is the main source of excitation of the nebula. Cappa et al. (2009) observed the ^{12}CO ($J = 1 \rightarrow 0$) and ($J = 2 \rightarrow 1$) lines using SEST data and ($J = 1 \rightarrow 0$) line using NANTEL data towards RCW 78. They found a CO ring-like structure in

the velocity range from -52.5 km s^{-1} to -43.5 km s^{-1} , which is almost coincident with the brightest western part of the nebula. A second CO structure in the velocity range from -43.5 km s^{-1} to -39.5 km s^{-1} was also detected. The molecular gas in a region $12' \times 10'$ centered on WR 55 shows similar characteristics in the line velocities to those of the ionized gas (Chu & Treffers 1981), i.e. larger negative velocities to the north, and more positive velocities close to the star. The authors suggest that WR 55 is not only responsible for the ionization at the surface of the molecular cloud, but also for the shape and kinematics of RCW 78. Infrared MSX, IRAS, and GLIMPSE data were also analyzed by these authors. They reported two small clusters of candidate young stellar objects (YSOs) centered on about RA, Dec(J2000) = $(13^{\text{h}}34^{\text{m}}15.0, -62^{\circ}26')$ ($l, b = 307^{\circ}52', 00^{\circ}02'$) and RA, Dec(J2000) = $(13^{\text{h}}35^{\text{m}}10, -62^{\circ}26')$ ($l, b = 307^{\circ}51', 00^{\circ}02'$). The positions of these clusters are coincident with two bright and extended infrared sources observed at $60 \mu\text{m}$ (referred to in that work as sources B and C, respectively). They also

claim that the expansion caused by WR 55 might have triggered the star formation disclosed by the presence of other candidate YSOs observed in the direction of the molecular gas in the velocity range from -56.5 km s^{-1} to -39.5 km s^{-1} .

Given the information above, we explore the physical and kinematical characteristics of the molecular gas in RCW 78. Is this nebula simply a non-expanding H α region? Is WR 55 interacting with the molecular and/or ionized gas of the nebula? How can the velocity gradient observed in the ionized and molecular gas be explained?

To perform a thorough study of the distribution of the molecular and ionized gas of RCW 78, as well as their physical and kinematical properties, optimal fully sampled and high velocity resolution ^{12}CO ($J = 1 \rightarrow 0$) observations covering a region of $\sim 25' \times 25'$ around the star WR 55 were carried out. The molecular observations were analyzed in conjunction with archival data of both radiocontinuum at 1.4 and 4.85 GHz, and H α observations to account for the ionized gas. The databases used in this work are outlined in Sect. 2, the results are described in Sect. 3, and our discussion given in Sect. 4. Conclusions are presented in Sect. 5. This is the first of a series of papers aimed at studying the characteristics of molecular gas around Wolf-Rayet ring nebulae.

2. Observations and data reduction

The databases used in this work are:

1. Intermediate angular-resolution, medium-sensitivity, and high-velocity resolution ^{12}CO ($J = 1 \rightarrow 0$) data obtained with the 4-m NANTEN millimeter-wave telescope of Nagoya University. At the time we carried out the observations in April 2001, this telescope was installed at Las Campanas Observatory, Chile. The half-power beamwidth and the system temperature, including the atmospheric contribution towards the zenith, were $2.6'$ ($\sim 3.8 \text{ pc}$ at 5 kpc) and $\sim 220 \text{ K}$ (SSB) at 115 GHz, respectively. The data were gathered using the position switching mode. Observations of points devoid of CO emission were interspersed among the program positions. The coordinates of these points were retrieved from a database that was kindly made available to us by the NANTEN staff. The spectrometer used was acousto-optical with 2048 channels providing a velocity resolution of $\sim 0.055 \text{ km s}^{-1}$. For intensity calibrations, a room-temperature chopper wheel was employed (Penzias & Burrus 1973). An absolute intensity calibration (Ulich & Haas 1976; Kutner & Ulich 1981) was achieved by observing Orion KL (RA(1950.0) = $5^{\text{h}}32^{\text{m}}47^{\text{s}}.0$, Dec (1950.0) = $-5^{\circ}24'21''$), and ρ Oph East (RA(1950.0) = $16^{\text{h}}29^{\text{m}}20^{\text{s}}.9$, Dec (1950.0) = $-24^{\circ}22'13''$). The absolute radiation temperatures, T_{R}^* , of Orion KL and ρ Oph East, which were both observed by the NANTEN radiotelescope, were assumed to be 65 K and 15 K, respectively (Moriguchi et al. 2001). The CO observations covered a region ($\Delta l \times \Delta b$) of $86.4' \times 86.4'$ centred at $(l, b) = (307.8, 0.16)$ and the observed grid consists of points located every $1.35'$ (full sampling). A total of 489 positions were observed. The integration time per point was typically 16 s resulting in an rms noise of $\sim 0.3 \text{ K}$. A second-order degree polynomial was subtracted from the observations to account for instrumental baseline effects. The spectra were reduced using CLASS software (GILDAS working group)¹.

¹ <http://www.iram.fr/IRAMFR/PDB/class/class.html>

2. Narrow-band H α data retrieved from the SuperCOSMOS H-alpha Survey (SHS)². The images have a sensitivity of 5 Rayleigh, and $\sim 1''$ spatial resolution (Parker et al. 2005).
3. Radio continuum observations:
 - 1.4 GHz data retrieved from the Southern Galactic Plane Survey (SGPS)³. The angular resolution is $100''$ and the rms sensitivity is below 1 mJy beam^{-1} (Haverkorn et al. 2006);
 - 4.85 GHz data retrieved from the Parkes-MIT-NRAO (PMN) Southern Radio Survey. The images have $\sim 5'$ resolution and $\sim 8 \text{ mJy beam}^{-1}$ rms noise plus confusion (Condon et al. 1993);
 - 843 MHz image retrieved from the Molonglo Galactic Plane Survey (MGPS)⁴. The angular resolution is $43'' \times 43''$ cosec(dec) and the rms sensitivity is $1-2 \text{ mJy beam}^{-1}$.
4. Infrared data at $24 \mu\text{m}$ (angular resolution $\sim 5''$) obtained from the Multiband Imaging Photometer for *Spitzer* (MIPS) from the MIPS Inner Galactic Plane Survey (MIPSGAL)⁵ (Carey et al. 2005).

3. Results and analysis of the observations

3.1. CO emission

Representative CO profiles obtained at different positions towards RCW 78 are shown in Fig. 2. The CO emission shows three main velocity components: *i*) ~ -58 to -46 km s^{-1} (profiles *a* to *g*), *ii*) ~ -44 to -38 km s^{-1} (profile *c*, and probably *d*), and *iii*) ~ -33 to -28 km s^{-1} (profiles *d*, *e*, and *g*).

It is noticeable from Fig. 3 that the molecular gas distribution is quite dissimilar among the three afore velocity ranges. In the velocity range from -58 km s^{-1} to -46 km s^{-1} (upper left panel of Fig. 3), the molecular gas displays a very clumpy ring-like structure that has an excellent morphologic correlation with the H α nebula, except for the lane of molecular gas between $(l, b) \approx (307^{\circ}54', +00^{\circ}09')$ and $(l, b) \approx (307^{\circ}52', -00^{\circ}02')$ (see Figs. 1 and 3, right panel) that has no H α counterpart. The velocities of the CO line are similar to those observed at H α by Chu & Treffers (1981). This molecular structure was reported by Cappa et al. (2009). In the second velocity range from -44 km s^{-1} to -38 km s^{-1} (middle left panel of Fig. 3), the CO emission is mostly confined to a region within $307^{\circ}45' < l < 308^{\circ}00'$ and $-00^{\circ}02' < b < +00^{\circ}12'$. This molecular structure, also reported by Cappa et al. (2009), shows no resemblance to the H α nebula. In the third velocity range from -33 km s^{-1} to -28 km s^{-1} (lower left panel of Fig. 3), the molecular gas appears as an elongated feature mostly confined along $b = +00^{\circ}05'$.

For the three molecular components, mean radial velocities weighted by line temperature (\bar{V}) were derived using

$$\bar{V} = \frac{\sum_i T_{\text{Peak}_i} \times V_{\text{Peak}_i}}{\sum_i T_{\text{Peak}_i}}, \quad (1)$$

where T_{Peak_i} and V_{Peak_i} are the peak temperature and the peak radial velocity of the i -spectrum obtained within the first contour level used in Fig. 3 for each molecular component. The mean

² <http://www-wfau.roe.ac.uk/sss/halpha/index.html>

³ <http://www.atnf.csiro.au/research/HI/sgps/queryForm.html>

⁴ <http://www.astrop.physics.usyd.edu.au/MGPS/>

⁵ <http://sha.ipac.caltech.edu/applications/Spitzer/SHA/>

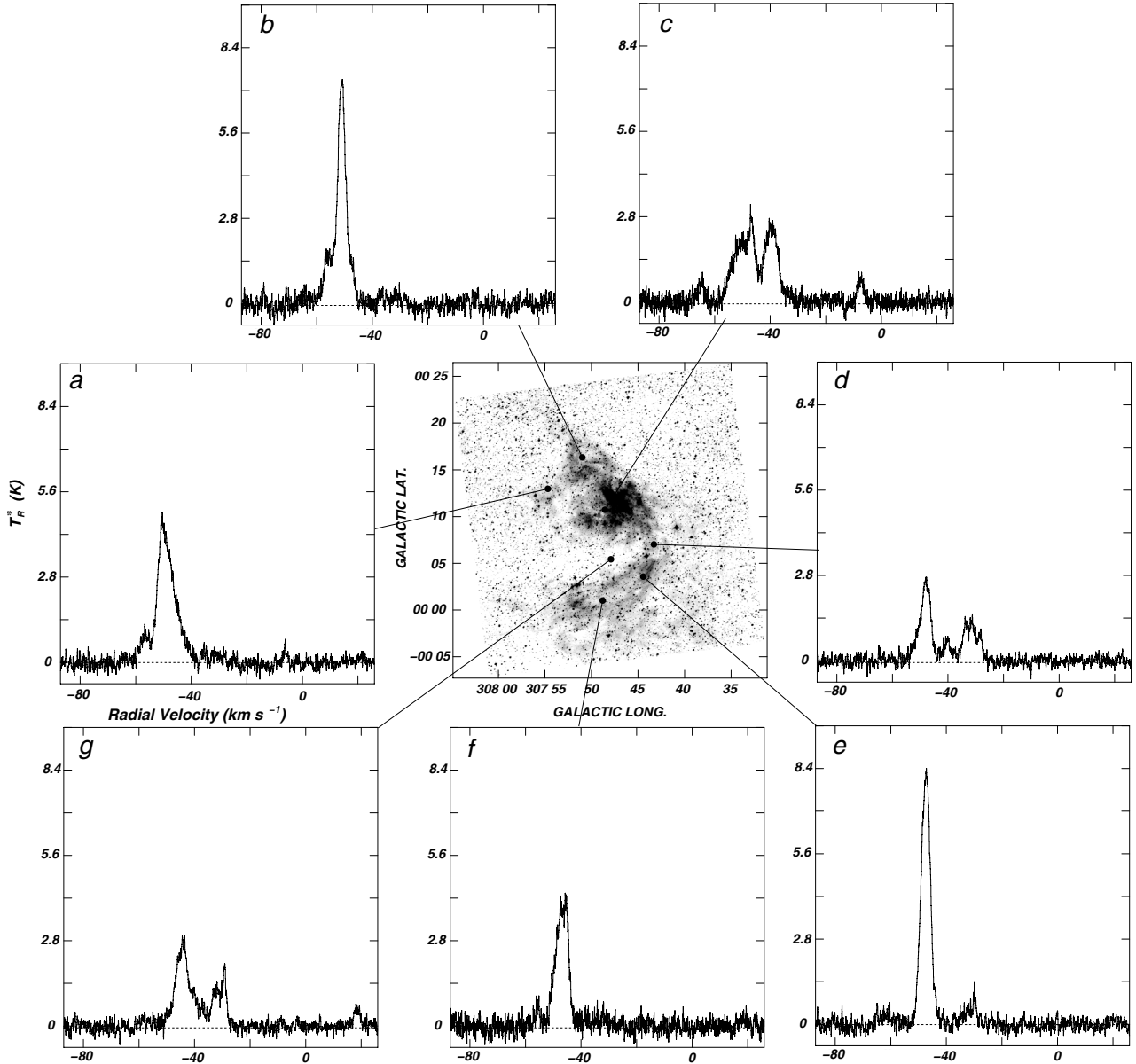


Fig. 2. Mean CO emission profiles toward seven regions of the RCW 78 nebula around the star WR 55. The CO profiles are averaged over a square area $\sim 3'$ in size, centered on the black dots drawn on the H α image (*center*). The profile units are T_R^* in K (ordinate) and V_{LSR} in km s^{-1} .

weighted radial velocities for the molecular gas in the three velocity ranges depicted in Fig. 3 are -49.5 km s^{-1} , -40.7 km s^{-1} , and -29.3 km s^{-1} , respectively. Using \bar{V} and the Galactic velocity field of Brand & Blitz (1993) along $l = 307^\circ 50'$, kinematical distances to the molecular features were derived. We point out that along this Galactic longitude, radial velocities more negative than -47.5 km s^{-1} are forbidden. Nonetheless, it is well-established that noncircular motions of the order of $\sim 8 \text{ km s}^{-1}$ (Burton & Gordon 1978) are known to exist in the Galaxy. Keeping this in mind, the molecular component at -49.5 km s^{-1} was assumed to be in the neighborhood of the tangential point at a distance of $\sim 5 \text{ kpc}$. This distance agrees with one of the quoted distance ranges of WR 55. On the basis of this distance agreement, and the excellent correspondence between the morphology and line velocities of the CO and H α emission, we believe that this molecular component is very likely related to both WR 55 and RCW 78. For the molecular component at -40.7 km s^{-1} , near and far kinematical distances of 3.5 kpc and 6.9 kpc are

derived. In Fig. 3 (middle right panel), we overlay this component onto the H α emission of RCW 78. Though the southern border of the CO feature appears to clearly delineate the inner boundary of the H α emission, providing evidence of a possible relationship, we suggest that this feature is very likely a background object of RCW 78. The visual extinction (A_v) at $(l, b) \approx (307^\circ 47', +00^\circ 09')$ can be obtained using the equation of Bohlin et al. (1978)

$$N(\text{H}_2)/A_v = 0.94 \times 10^{21} (\text{cm}^{-2} \text{ mag}^{-1}), \quad (2)$$

where $N(\text{H}_2)$ is the molecular-hydrogen column-density (see below). We obtain in this direction, a value of $N(\text{H}_2) \sim 4 \times 10^{21} \text{ molecules cm}^{-2}$, which implies $A_v \sim 4 \text{ mag}$. Bearing in mind this figure, the visual absorption that should arise from the molecular gas is not noticed in the brightness of the optical nebula. Therefore, we suggest that this object is unrelated to RCW 78 and is located at the far kinematical distance. On the other hand, the CO feature at -29.3 km s^{-1}

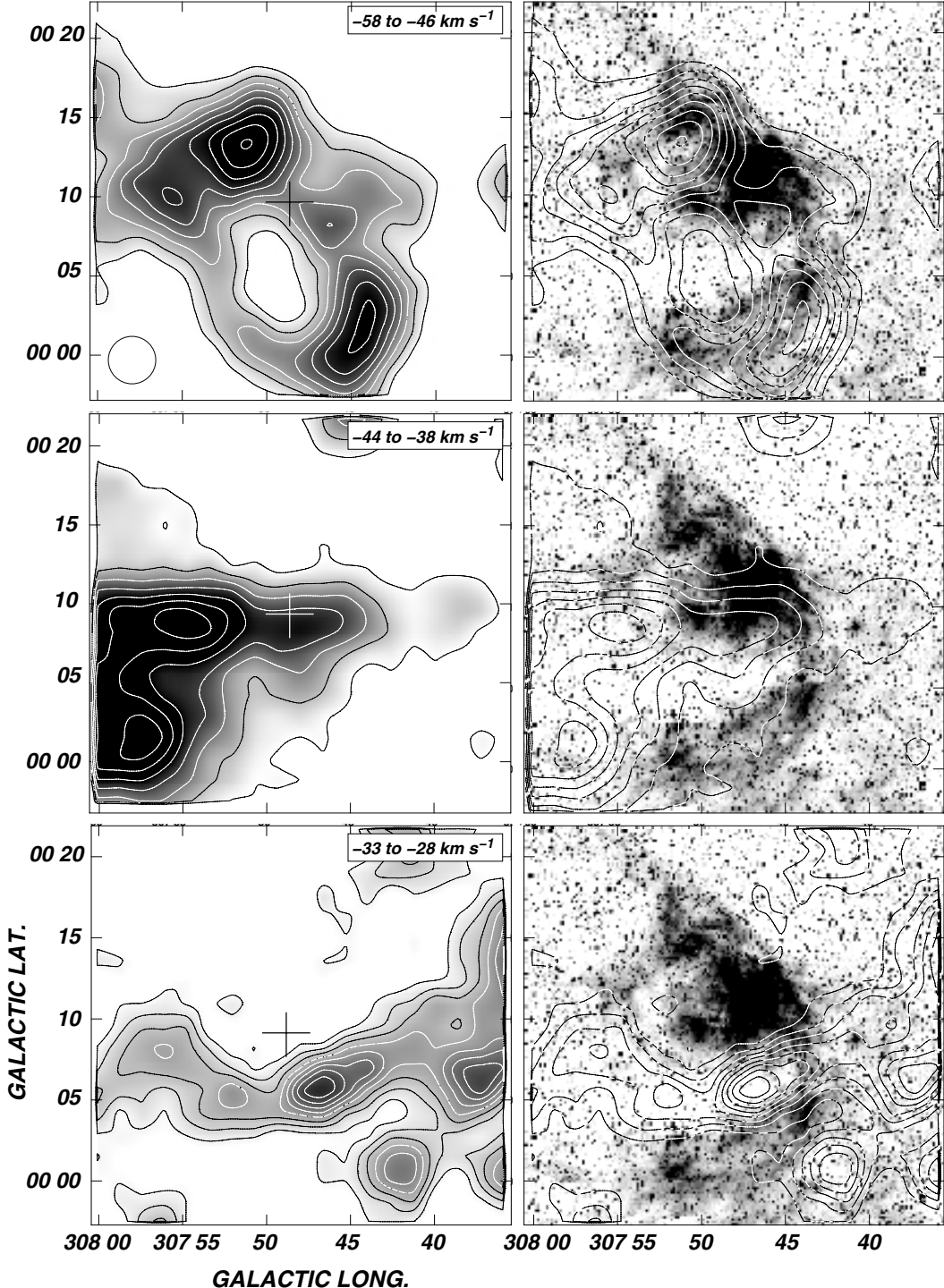


Fig. 3. Left panels: spatial distribution of CO emission in three velocity ranges. The velocity range is given in the upper right corner of each map. The line temperature is averaged over the corresponding velocity range. In the velocity range ~ -58 to -46 km s $^{-1}$, the lowest contour is 0.5 K (~ 20 rms) and the contour spacing is 0.35 K. In the velocity range -44 to -38 km s $^{-1}$, the lowest contour is 0.35 K (~ 14 rms) and the contour spacing is 0.7 K. In the velocity range -33 to -28 km s $^{-1}$, the lowest contour is 0.42 K (~ 11 rms) and the contour spacing is 0.21 K. In all cases, the greyscale goes from 0.35 to 3.15 K. The position of WR 55 is marked by a plus sign at the center of each image. The beam size of the CO observations is shown by a circle in the *upper left panel*. Right panels: overlay of the mean CO emission (contours) in the three velocity ranges and the SHS H α emission of RCW 78 (grey scale).

(Fig. 3, lower panel) shows an excellent spatial correlation with the high optical absorption lane seen at $b \approx +00^\circ 05'$ between $307^\circ 44' < l < 307^\circ 55'$. Based on this, we suggest that this feature is a foreground object of RCW 78, locating it at its near kinematical distance (~ 2.8 kpc). Based on the above, from here

onwards we concentrate on the analysis of the molecular gas distribution observed between -58 km s $^{-1}$ and -44 km s $^{-1}$, which is the only one likely to be associated with RCW 78.

In Fig. 4, a collection of narrow velocity images depicting the CO spatial distribution in the velocity range from

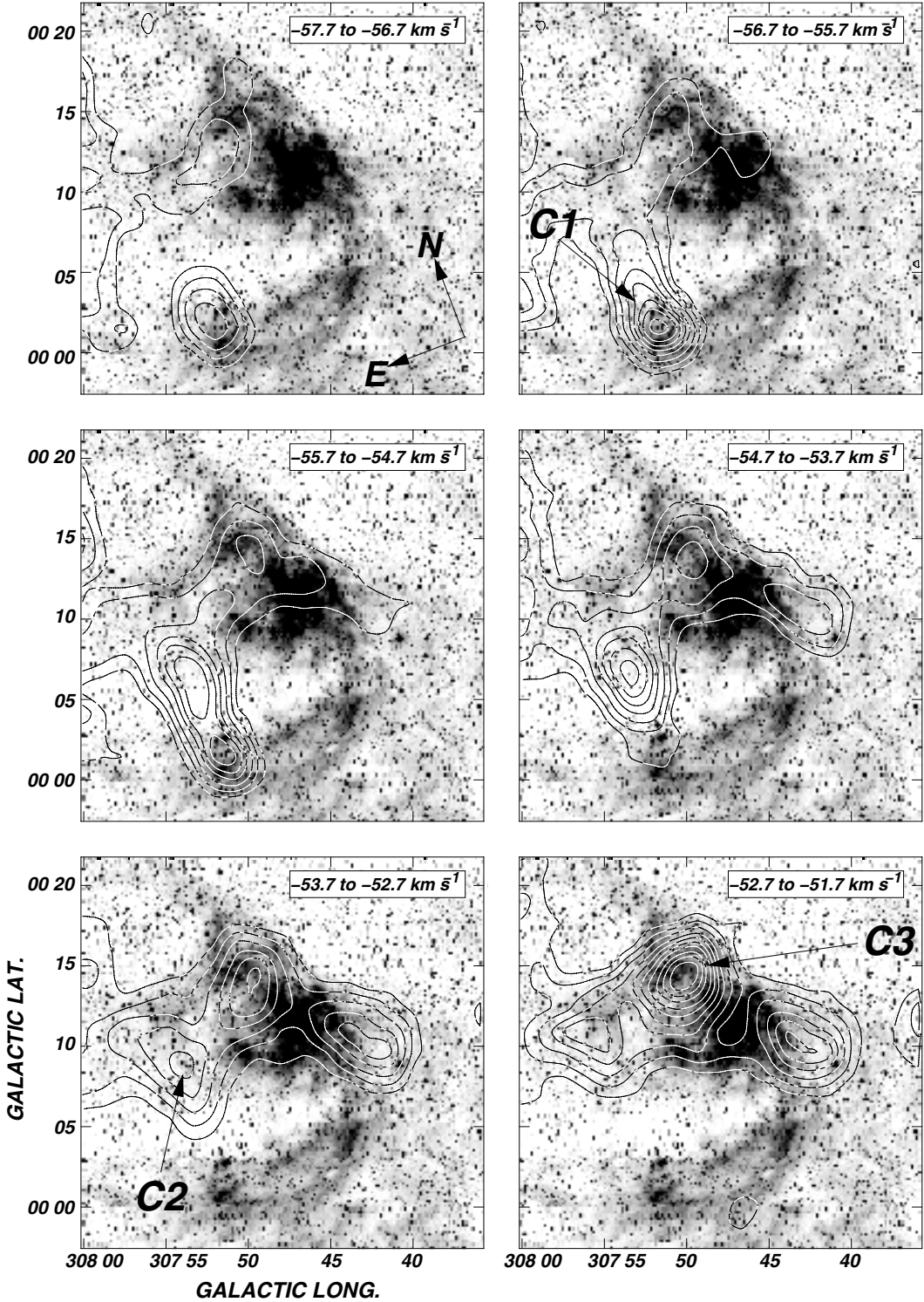
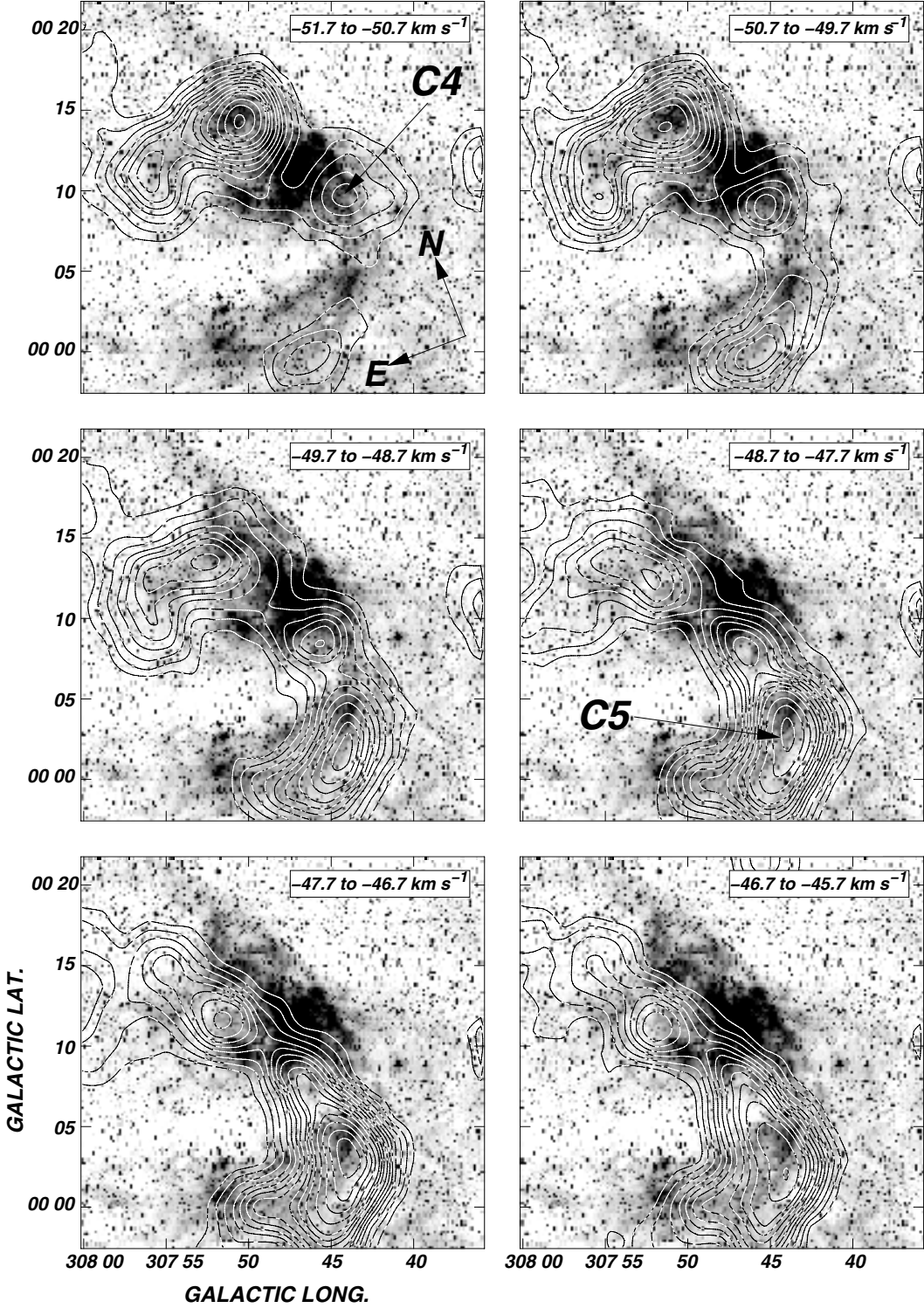


Fig. 4. Overlay of the mean CO emission (contours) in the velocity range from ~ -57.7 to -45.7 km s^{-1} and the SHS H α emission of RCW 78 (grey scale). The velocity interval of each map is indicated in the upper right corner of each image. The orientation of the equatorial coordinate system is given by the thick arrows labeled E (east) and N (north) at the first map. The lowest temperature contour is 0.8 K ($\sim 10 \text{ rms}$). The contour spacing temperature is 0.6 K.

-57.7 km s^{-1} to -45.7 km s^{-1} is shown. Every image represents an average of the CO emission over a velocity interval of 1 km s^{-1} (20 individual channel maps). The CO emission distribution shown in Fig. 4 (in contours) is projected onto the SHS H α image of RCW 78 (greyscale). The velocity interval of the individual images is indicated in the upper right corner.

For the sake of further analysis, five molecular concentrations are identified. They are labelled from C1 to C5 in order of increasing radial velocity. Concentration C1, whose maximum is at $(l, b) \approx (307^{\circ}53', 00^{\circ}03')$, is visible from -57.7 to -54.7 km s^{-1} attaining a maximum emission temperature of $\sim 4.8 \text{ K}$. This feature appears projected onto the region where

**Fig. 4.** continued.

HD 117797 and the open cluster C1331-622 are located. This region is also coincident with the area where candidate YSOs were reported by [Cappa et al. \(2009\)](#). At slightly more positive velocities, the concentration C2 is found. This feature is first detected in the velocity interval from -56.7 km s^{-1} to -55.7 km s^{-1} as an extension of C1 along the position angle of $\sim 45^\circ$. Towards more positive velocities, the peak emission of this feature is shifted towards slightly higher longitudes and latitudes. In the velocity range from -52.7 km s^{-1} to -48.7 km s^{-1} ,

C2 has a very good spatial correlation with the faint H α emission seen in the northeastern part of RCW 78, at $l > 307^\circ 50'$. Concentration C3 spans the velocity range from -55.7 km s^{-1} to -48.7 km s^{-1} and has a very good morphological correlation with the H α emission of RCW 78 seen 5' northwards of WR 55. This component reaches a maximum emission temperature of 7.7 K at $(l, b) \approx (307^\circ 50', 00^\circ 14')$ in the velocity range from -51.7 km s^{-1} to -50.7 km s^{-1} . The concentration C4 becomes noticeable in the velocity range from -55.7 km s^{-1} to

Table 1. Main physical parameters of the molecular concentrations C1, C2, C3, C4, and C5.

Parameter	C1	C2	C3	C4	C5
Angular size (')	~5	~10	~9	~7	~13
Linear size (pc)	5.6 [†]	14.5 [‡]	13 [‡]	10.2 [‡]	19 [‡]
\bar{V} (km s ⁻¹)	-56.1 ± 0.2	-52.8 ± 1.6	-49.8 ± 1.3	-49.4 ± 1.2	-47.1 ± 0.9
$\Delta\bar{V}$ (km s ⁻¹)	2.8 ± 0.5	5.1 ± 1.1	8.2 ± 2.3	5.1 ± 1.1	4.7 ± 0.9
\bar{T}_{peak} (K)	3.1 ± 0.9	3.9 ± 0.5	4.8 ± 1.2	4.1 ± 0.8	5.4 ± 1.1
N_{H_2} (10 ²¹ cm ⁻²)	0.9 ± 0.2	3.3 ± 0.5	4.0 ± 0.6	2.2 ± 0.3	3.9 ± 0.7
M_{tot} (10 ³ M_{\odot})	0.6 ± 0.2 [†]	6.8 ± 2.9 [‡]	8.7 ± 3.4 [‡]	4.2 ± 1.6 [‡]	13.8 ± 5.5 [‡]
n_{H_2} (cm ⁻³)	16 ± 5	118 ± 50	108 ± 42	91 ± 34	101 ± 41
\bar{T}_{exc} (K)	7.6	8.9	10.2	9.4	11.1

Notes. ^(†) Considering a distance of 3.9 kpc (see Sect. 4.1). ^(‡) Considering a distance of 5 kpc (see Sect. 3.1).

-54.7 km s⁻¹ as a weak feature projected onto the low Galactic longitude extreme of RCW 78. This feature remains clearly visible as a separate feature up to velocities of -47.7 km s⁻¹. At more positive velocities, this concentration is very difficult to follow because it merges with the northernmost extreme of C5. The latter is first observed in the velocity range from -51.7 km s⁻¹ to -50.7 km s⁻¹ as a detached CO emission feature seen projected slightly offset from the H α southernmost extreme of RCW 78. Concentration C5 reaches a maximum temperature of 8.9 K at (l, b) ≈ (307°44', 00°03') in the velocity interval from -47.7 km s⁻¹ to -46.5 km s⁻¹.

In Table 1, we list some physical and geometrical properties of the molecular concentrations from C1 to C5. The angular and linear sizes of the concentrations are listed in rows 1 and 2, respectively. Figure 4 shows that a velocity gradient is present among the five molecular concentrations. In Table 1, the average velocity (\bar{V}), width ($\Delta\bar{V}$), and peak temperature \bar{T}_{peak} , obtained from a gaussian fitting to the mean CO profile of each molecular concentration, are given in rows 3, 4, and 5, respectively. To obtain these profiles, all individual CO spectra within the 0.5 K contour level in Fig. 3 were added up and averaged. The mean velocity of the concentrations clearly increases from C1 to C5. This velocity gradient is also noticeable in the velocity-Galactic longitude image shown in Fig. 5. This image shows the averaged CO emission in the Galactic longitude range 307°42' < l < 308°00'. The concentrations C1, C2, C3, C4, and C5 are identified.

The mass of the molecular gas was derived using the empirical relationship between the molecular hydrogen column density, $N(\text{H}_2)$, and the integrated molecular emission, $I_{^{12}\text{CO}}$ ($\equiv \int T_{\text{R}}^* dv$). The conversion between $I_{^{12}\text{CO}}$ and $N(\text{H}_2)$ is given by the equation

$$N(\text{H}_2) = (1.9 \pm 0.3) \times 10^{20} I_{^{12}\text{CO}} \quad (\text{cm}^{-2}) \quad (3)$$

(Digel et al. 1996; Strong & Mattox 1996). The total molecular mass M_{tot} was calculated through

$$M_{\text{tot}} = (m_{\text{sun}})^{-1} \mu m_{\text{H}} \sum \Omega N(\text{H}_2) d^2 (M_{\odot}), \quad (4)$$

where m_{sun} is the solar mass ($\sim 2 \times 10^{33}$ g), μ is the mean molecular weight, which is assumed to be equal to 2.8 after allowance of a relative helium abundance of 25% by mass (Yamaguchi et al. 1999), m_{H} is the hydrogen atom mass ($\sim 1.67 \times 10^{-24}$ g), Ω is the solid angle subtended by the CO feature in ster, d is the distance expressed in cm, and M_{tot} is given in units of solar masses. Values of $N(\text{H}_2)$, M_{tot} , and molecular volume density (n_{H_2}) for each molecular concentration are quoted in rows 4–6 of Table 1, respectively.

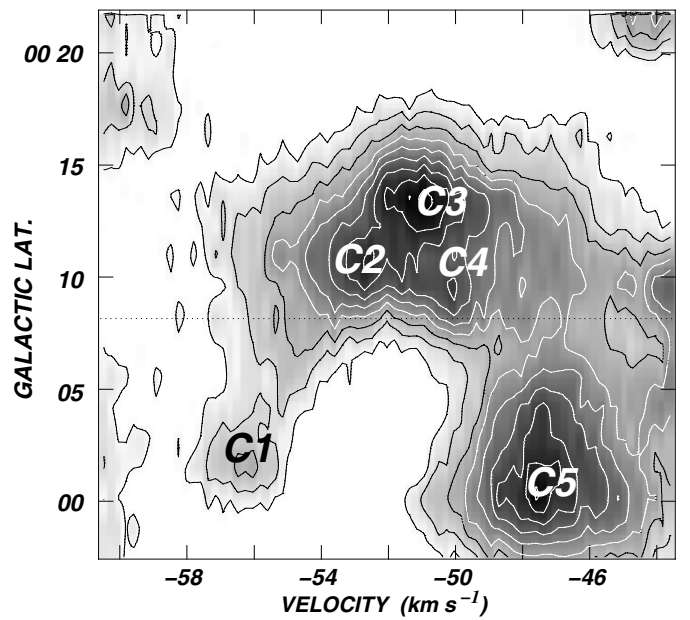


Fig. 5. Galactic latitude-velocity contour map of the average CO emission in the Galactic longitude range from 307°40' to 308°00'. The lowest temperature contour is 0.5 (~3.5 rms). The contour spacing is ~0.3 K. The location of WR 55 is indicated by the dotted line.

To probe the surface conditions of the molecular gas, we calculated mean excitation temperatures (\bar{T}_{exc}). Assuming ^{12}CO emission to be optically thick, the average excitation temperatures were obtained from

$$\bar{T}_{\text{peak}}(^{12}\text{CO}) = J_{\nu}(\bar{T}_{\text{exc}}) - J_{\nu}(T_{\text{bg}}), \quad (5)$$

(Dickman 1978) where J_{ν} is the Planck function at a frequency ν , and T_{bg} is the background temperature (~2.7 K). These values are presented in row 7 of Table 1. We note that Eq. (5) assumes a filling factor of unity, which implies that the values of T_{exc} quoted in Table 1 must be considered as lower limits.

3.2. Radio continuum emission

The radio continuum emission distribution at 1.4 GHz obtained from the ATCA archives is shown in the upper left panel of Fig. 6. Regardless of the difference between the angular resolution and that of the SuperCOSMOS image, the radio-continuum emission distribution resembles the H α emission of the nebula (see Fig. 6, left lower panel). Two intense features, which have no counterparts in the optical emission of RCW 78, are seen

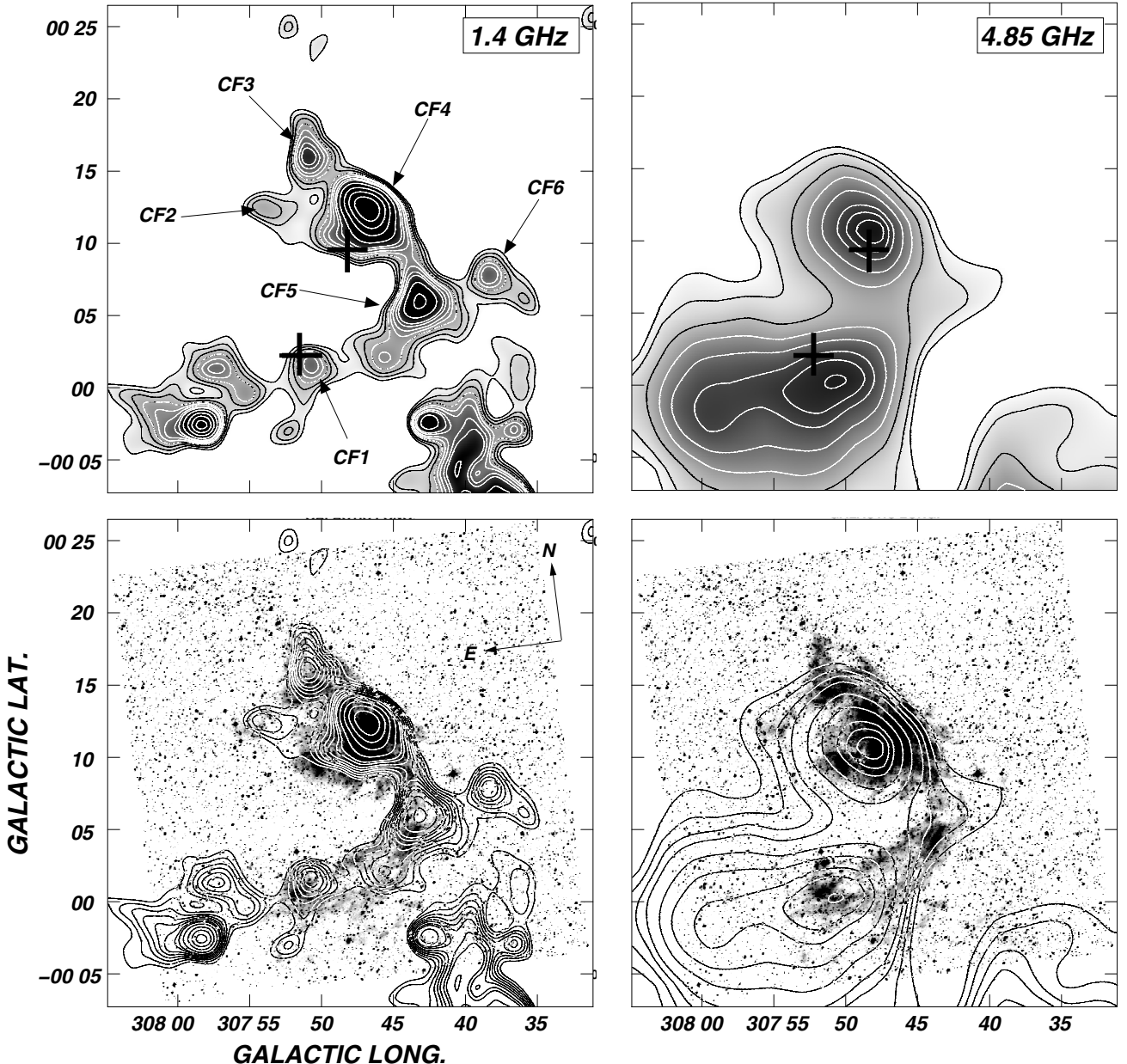


Fig. 6. Upper panels: radio continuum emission distribution at 1.4 GHz (left panel) and 4.85 GHz (right panel). Contour levels for the 1.4 GHz image go from 21 mJy beam^{-1} to 42 mJy beam^{-1} in steps of 7 mJy beam^{-1} and from 60 mJy beam^{-1} to 80 mJy beam^{-1} in steps of 10 mJy beam^{-1} . For the 4.85 GHz data the lowest contour level is 40 mJy beam^{-1} and the contour spacing is 20 mJy beam^{-1} . Black crosses indicate the positions of WR 55 and HD 117797. Lower panel: overlay of the radiocontinuum emission at 1.4 GHz and 4.85 GHz on the $\text{H}\alpha$ emission of RCW 78.

toward the south and southeast of the optical nebula. The southern feature located in the region between $307^{\circ}35' < l < 307^{\circ}45'$ and $-0^{\circ}06' < b < 0^{\circ}02'$ is probably related to an intense radio-continuum source located at $(l, b) = (307^{\circ}37', -0^{\circ}18')$ (not shown here), while the southeastern feature located in a region between $307^{\circ}55' < l < 308^{\circ}05'$ and $-0^{\circ}05' < b < 0^{\circ}02'$ is likely related to the source IRAS 13316-6210. These features are considered no further in our analysis.

Six intense features peaking at about $(l, b) = (307^{\circ}51', 0^{\circ}02')$, $(l, b) = (307^{\circ}54', 0^{\circ}12')$, $(l, b) = (307^{\circ}51', 0^{\circ}16')$, $(l, b) = (307^{\circ}47', 0^{\circ}13')$, $(l, b) = (307^{\circ}44', 0^{\circ}06')$, and $(l, b) = (307^{\circ}38', 0^{\circ}08')$ are seen projected onto the optical nebula. In terms of their positions and the molecular concentrations described in Sect. 3.1, these features are referred to as CF1, CF2, CF3, CF4, CF5, and CF6, respectively. To determine their radio-continuum flux densities at 1.4 GHz ($S_{1.4}$), the emission

distribution was analyzed using of the NOD2 package (Haslam 1974). We calculated the values of $S_{1.4}$ for each feature, after subtracting a background emission, and summarize these values in Table 2. The error quoted for $S_{1.4}$ stems from the uncertainty in the first contour level used to define the sources.

To characterize the nature of the radio continuum emission arising from RCW 78, the 4.85 GHz image obtained from the PMN Southern Radio Survey (Fig. 6, upper right panel) was also analyzed. Though a detailed comparison between the 4.85 GHz and the $\text{H}\alpha$ emission is difficult owing to the difference in angular resolution, two different features at 4.85 GHz, peaking at about $(l, b) = (307^{\circ}48', 0^{\circ}11')$ and $(l, b) = (307^{\circ}51', 0^{\circ}01')$, seem to be morphologically correlated with the optical nebula. The first of them appears to be projected onto the brightest region of the optical nebula and its first contour level engulfs CF2, CF3, CF4, CF5, and CF6. As expected, the intense

Table 2. Radio continuum parameters of continuum features CF1, CF2, CF3, CF4, CF5, and CF6 derived from the 1.4 GHz emission.

	CF1	CF2	CF3	CF4	CF5	CF6
$S_{1.4}$ (mJy)	23 ± 7	21 ± 7	55 ± 8	287 ± 21	131 ± 25	27 ± 8
Peak position (l, b)	$307^{\circ}51', 0^{\circ}02'$	$307^{\circ}54', 0^{\circ}12'$	$307^{\circ}51', 0^{\circ}16'$	$307^{\circ}47', 0^{\circ}13'$	$307^{\circ}44', 0^{\circ}06'$	$307^{\circ}38', 0^{\circ}08'$
T_b (K)	2.4	1.9	3.0	5.9	4.1	2.5
EM (10^3 pc cm $^{-6}$)	1.5	1.2	1.9	3.7	2.6	1.6
n_e (cm $^{-3}$)	$21 \pm 7^{\ddagger}$	$20 \pm 6^{\ddagger}$	$21 \pm 6^{\ddagger}$	$20 \pm 5^{\ddagger}$	$22 \pm 6^{\ddagger}$	$20 \pm 5^{\ddagger}$

Notes. (\ddagger) Considering a distance of 5 kpc (see text). (\dagger) Considering a distance of 3.9 kpc (see Sect. 4.1).

emission at 4.85 GHz arises from the central part of the nebula, toward the region of CF3 and CF4. The 4.85 GHz emission counterpart of CF2 is the low brightness elongation seen around $(l, b) \approx (307^{\circ}54', +00^{\circ}13')$, while the counterpart corresponding to both CF5 and CF6 is the low intensity sharp-pointed structure observed around $(l, b) \approx (307^{\circ}43', +00^{\circ}07')$. The morphological correspondences described above can be more clearly visualized after convolving the 1.4 GHz image down to the angular resolution of the 4.85 GHz image (not shown here). The continuum flux density measured for this feature is $S_{4.85} = 440 \pm 50$ mJy. To obtain the spectral index towards this region, the flux density at 1.4 GHz of features CF2, CF3, CF4, CF5, and CF6 were added up. These values provide a spectral index of $\alpha = -0.14 \pm 0.05$, which is compatible with the optically thin regime of an HII region.

The second feature detected at 4.85 GHz is seen projected onto HD 117797 and very likely represents the 4.85 GHz counterpart of CF1. Unfortunately, the angular resolution of these observations makes it almost impossible to isolate this feature from the near-by emission structure peaking approximately at $(l, b) \approx (307^{\circ}58', -00^{\circ}02')$. This prevents us from deriving a reliable continuum flux density at this frequency. The radio continuum image at 843 MHz retrieved from MGPS (not shown here) do not show instrumental artifacts in the area of CF1. Using this survey, we derived for CF1 at this frequency a flux density of 24 ± 5 mJy. Using this value and the 1.4 GHz flux density quoted from CF1 in Table 2, a spectral index of $\alpha = -0.08 \pm 0.15$ is derived. The spectral index is compatible again, within the errors, with free-free emission of an HII region in the optically thin regime. This speaks in favour of interpreting CF1 as the HII region created by the early-type star HD 117797.

The emission measure ($EM = \int n_e^2 dl$) of an HII region can be obtained via the relationship between optical depth at a frequency ν (τ_ν) and T_b given by

$$T_b = T_e \times (1 - e^{-\tau_\nu}) \quad (\text{K}), \quad (6)$$

where T_e is the electron temperature (considered to be $\sim 10^4$ K), and the optical depth (τ_ν) is given by

$$\tau_\nu = 0.08235 T_e^{-1.35} \nu^{-2.1} EM. \quad (7)$$

In Eq. (7), ν is given in GHz and EM in pc cm $^{-6}$. Using the radio continuum emission at 1.4 GHz, values of EM were calculated for each feature. These values are shown in row 4 of Table 2. Assuming pure hydrogen plasma, adopting an extent along the line of sight equal to the observed minor axis, and using the EM values determined before, the electron densities (n_e) were calculated. These values are quoted in row 5 of Table 2.

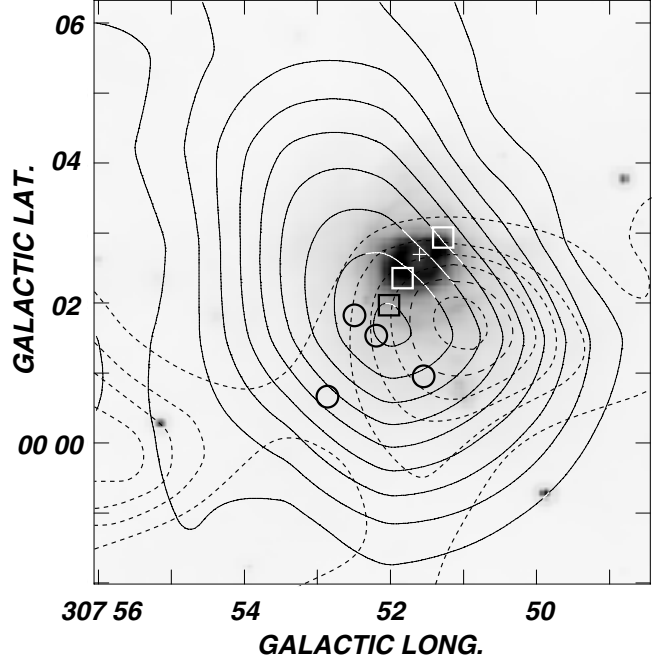


Fig. 7. Overlay of the MIPSGAL 24 μ m emission (greyscale) superimposed on the mean CO emission in the velocity interval from -57.7 to -54.7 km s $^{-1}$ (solid contours), and the 1.4 GHz emission (dashed contours). The position of HD 117797 is indicated with the white cross. The MSX and GLIMPSE candidate YSOs reported by Cappa et al. (2009) are indicated with squares and circles, respectively.

4. Discussion

4.1. Concentration C1

A look at Table 1 shows that the mean CO line width ($\bar{\Delta}V$), the molecular column density (N_{H_2}), the total mass (M_{tot}), and volume density (n_{H_2}) of concentration C1 are systematically lower than the corresponding physical parameters of the other CO concentrations. That its mean line width is on average almost half of the line width of the other concentrations may indicate that its dynamical state is different. In Fig. 7, we show the MIPSGAL 24 μ m emission of a $\sim 8' \times 8'$ region centered on HD 117797 and superimposed on both the mean CO emission in the velocity interval from -57.7 to -54.7 km s $^{-1}$ (concentration C1) and radio-continuum emission at 1.4 GHz of CF1. This image shows that the star HD 117797 and the HII region CF1 are seen projected onto the molecular concentration C1 and that HD 117797 appears to be projected close to the centre of CF1. In the same figure, a series of candidate YSOs reported by Cappa et al. (2009) are also seen in projection onto C1. On the basis of above, we may speculate that C1 is a molecular concentration that: a) is

being partially ionized by HD 117797; and b) may be experiencing a star-forming process, revealed by the presence of candidate YSOs.

To check the first assumption, we calculate the total number of Lyman continuum photons (N_ν) needed to keep CF1 ionized using

$$N_\nu = 0.76 \times 10^{47} T_4^{-0.45} \nu^{0.1} S_\nu d^2, \quad (8)$$

(Chaisson 1976), where T_4 is the electron temperature in units of 10^4 K, ν is the frequency in units of GHz, d is the distance in kpc, and S_ν is the total flux density in Jy. Substituting the appropriate values into Eq. (8), we obtain $N_\nu \approx 3 \times 10^{46} \text{ s}^{-1}$. This number is a lower limit to the total number of Lyman continuum photons required to maintain the gas ionized, since about 50% of the UV photons are absorbed by dust mixed with the gas in the HII region (Inoue 2001). Therefore, the number of Lyman continuum photons needed to power CF1 could be provided by HD 117797, since this number is a small fraction of the total ionizing photons emitted by a O8I star ($\sim 1 \times 10^{48} \text{ s}^{-1}$) (Martins et al. 2005).

A noticeable feature in Fig. 7 is a ringlike structure $\sim 1'$ diameter centered on the position of HD 117797, as seen in $24\mu\text{m}$ emission. The MIPSGAL image allowed us to conclude that the observed IR emission detected by Cappa et al. (2009) in this direction (source “B”) arises from this feature.

If HD 117797 were the powering source of the HII region CF1 and the latter associated with the molecular concentration C1, then the distance of this complex would be the distance to the star, namely 3.9 ± 1.0 kpc. If the star WR 55 and its associated nebula RCW 78 were close to the values determined by Chu & Treffers (1981) and van der Hucht (2001), namely around 6–7.6 kpc, then there would be no relationship between HD 117797 and WR 55. In turn, this implies that the molecular concentration C1 and the HII region CF1 are not related to RCW 78 and its associated molecular and ionized gas. On the other hand, if the distance to WR 55 were close to the estimates of Georgelin et al. (1988), namely 4 kpc, a physical association with HD 117797 (and its associated molecular and ionized gas) could not be ruled out. More accurate distance determinations to WR 55 and HD 117797 are necessary to shed some light on this issue.

4.2. A simple scheme for the molecular gas associated with RCW 78

In an attempt to explain the morphology and radial velocity of the remaining molecular concentrations (C2, C3, C4, and C5), a simple geometrical model was elaborated taking into account the following constraints: 1) the morphology of the molecular gas; 2) the velocity gradient exhibited by the molecular gas; 3) the angular distribution of the different CO concentrations; and 4) the morphology of the $H\alpha$ emission.

Since massive stars are born deeply buried within dense molecular clouds, the classical IB scenario predicts that the molecular gas should expand spherically around the star. Under the assumption of a spherically symmetric expansion, a shell with a central velocity V_0 and an expansion velocity V_{exp} should depict in a position-position diagram a “disk-ring” pattern when observed at different velocities. At V_0 , the shell should attain its maximum diameter, while at extreme velocities (either approaching or receding) the molecular emission should resemble a disk. At intermediate velocities, the radius of the ring shrinks as the extreme velocity is approached. According to Fig. 4, this

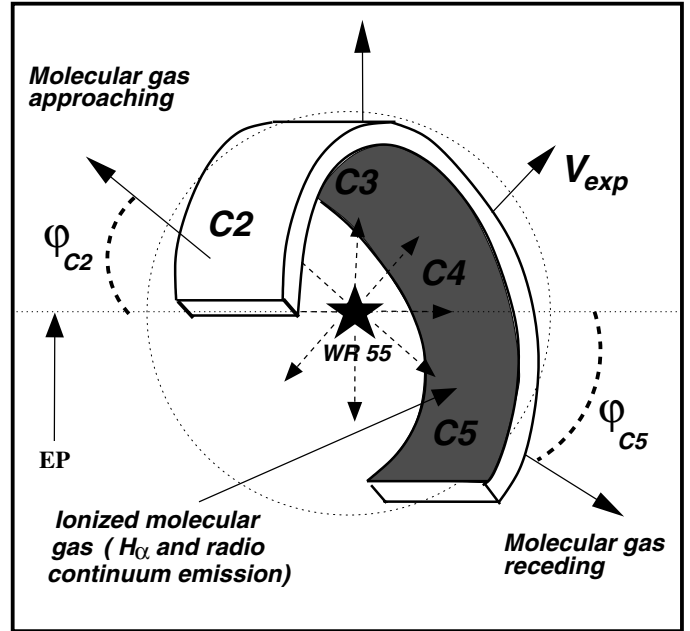


Fig. 8. Sketch of the model used to explain the spatial distribution and velocity of MB. The equatorial plane (EP) is depicted by the horizontal dotted line.

behaviour is not observed in our CO observations, which disagrees with the IB model.

Concentrations C2 to C5 can instead be explained by an spherically expanding ring-like structure partially surrounding WR 55, and tilted with respect to the plane of the sky. A sketch of this model is given in Fig. 8 where the approximate location of the different CO concentrations is given. The expansion of the molecular gas (filled arrows) is revealed by the velocity gradient (see Fig. 5). The ultimate cause of the expanding molecular gas are the stellar winds (dashed line arrows) of WR 55. From here onwards, the structure composed of concentrations C2, C3, C4, and C5 are labelled the molecular belt (or MB for short). To facilitate further analysis, we divided MB into two hemispheres with a plane that contains both the WR star and the observer (equatorial plane). This plane (dubbed EP for short) is also shown in Fig. 8.

Under the assumption that MB is expanding with respect to WR 55 with a velocity V_{exp} , the observed radial velocity is determined by two angles θ and φ . The former represents the inclination of MB with respect to the plane of the sky, whilst φ represents the angle between V_{exp} and the plane EP (see Fig. 8). We note that θ is single valued, whilst φ can take any value between 0° and 360° . For the sake of clarity, only the φ angles for concentrations C2 (φ_{C2}) and C5 (φ_{C5}) are shown in Fig. 8. On the basis of the sketch shown in Fig. 8, concentration C2 is approaching the observer (hence should have the most negative radial velocity), and concentration C5 is moving away from the observer (and should have the most positive radial velocity). The other molecular concentrations (C3 and C4) should have intermediate values of radial velocity. A rough estimate of the angle θ can be obtained from the observed distribution of the molecular gas, bearing in mind that a ring-like structure in space will become an elliptical feature when projected onto the sky plane. In Fig. 9, the ring-like distribution of our model is projected onto both the observed CO distribution in the velocity range from -54 to -46 km s^{-1} and the $H\alpha$ image of RCW 78. The approximate semi-major/semi-minor axis ratio (B/A) of the elliptical

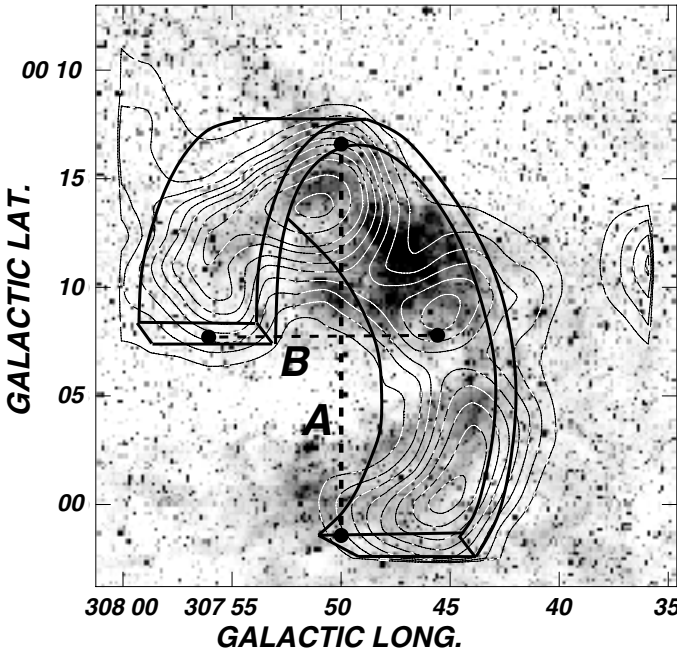


Fig. 9. Overlay of the model proposed for MB (broad contours) on the molecular gas in the velocity range from -54 km s^{-1} to -46 km s^{-1} (narrow contours) around the nebula RCW 78. The semi-major and semi-minor axes of MB (see text) are indicated by A and B, respectively.

structure provides an estimate of θ in terms of the trigonometric relation $B/A \approx \cos \theta$. A value of $B/A \approx 0.5$ can be obtained, which leads to $\theta \sim 60^\circ$.

According to Fig. 8, the maximum radial velocity difference among the molecular gas concentrations belonging to MB (ΔV_{MB}), is given by the radial velocity difference between the concentrations C2 (V_{C2}) and C5 (V_{C5}). From Table 1, $\Delta V_{\text{MB}} = V_{\text{C2}} - V_{\text{C5}} \approx 6 \text{ km s}^{-1}$. Based in our model,

$$\Delta V_{\text{MB}} = V_{\text{exp}} \times \sin(\theta) \times [\cos(\varphi_{\text{C5}}) + \cos(\varphi_{\text{C2}})]. \quad (9)$$

Using a coarse approximation $\varphi_{\text{C2}} \approx \varphi_{\text{C5}}$ (see Fig. 8), Eq. (9) can be written as

$$\Delta V_{\text{MB}} = 2 \times V_{\text{exp}} \times \sin(\theta) \times \cos(\varphi_{\text{C2}}). \quad (10)$$

Based on Fig. 8, we assumed that $\varphi_{\text{C2}} \approx 45^\circ$. Admittedly, the uncertainty in φ_{C2} can be very large. Inserting the appropriate values of θ and φ_{C2} into Eq. (10), we obtain $V_{\text{exp}} \approx 5 \text{ km s}^{-1}$. The main physical and geometrical properties of MB are listed in Table 3. The kinetic energy (E_{kin}) and momentum (P) were obtained by considering an expansion velocity of $\sim 5 \text{ km s}^{-1}$.

The proposed model is able to explain the main features of the optical nebula. The inner face of MB, which is exposed to the far-UV radiation field of WR 55, may be ionized. This ionized layer gives rise to both the radio continuum and H α emission. Since concentration C2 is located between the observer and the ionized gas, it diminishes the intensity of the H α emission that arises from the region of MB facing WR 55. On the other hand, since towards concentrations C3, C4, and C5 the observer is directly viewing the inner ionized layer of MB, the H α emission of these regions is not absorbed by the molecular gas. Since concentrations C3 and C4 may be closer to WR 55 than both C2 and C5, the intensity of both the H α and radio continuum emission is expected to be stronger there.

Though the proposed model is very simple, it is able to explain in a reasonable way the main observed characteristics of

Table 3. Main geometrical and physical parameters of MB.

Parameter	Value
Semi-major axis ('')	~ 9
Semi-minor axis ('')	~ 4.5
Semi-major axis (pc)	~ 13
ΔV_{MB} (km s^{-1})	~ 6
V_{exp} (km s^{-1})	~ 5
V_{syst} (km s^{-1})	-51
M_{tot} ($10^4 M_{\odot}$)	3.4 ± 1.3
E_{kin} (10^{48} erg)	~ 9
P ($10^4 M_{\odot} \text{ km s}^{-1}$)	~ 1.7

the H α , radio continuum, and molecular gas associated with RCW 78. Furthermore, the velocity gradient exhibited by the CO and H α is also nicely accounted for.

More elaborate models certainly are needed to improve our understanding of the origin and evolution of WRRN. Molecular ring-like structures have been reported previously around several massive stars. Beaumont & Williams (2010) surveyed the CO (3–2) line towards 43 identified *Spitzer* bubbles in the Galactic plane. They concluded that the molecular gas tends to lie in rings, rather than shells. The authors suggest that the parental molecular clouds, in which the massive stars and IBs are formed, are oblate with a dimension of a few parsecs in thickness. Expanding bubbles then break out of the parental molecular cloud and only a circular or elliptical ring of CO emission is detected, depending on the orientation of the axis. The authors claimed that if the wind emitted by the star powering the bubble is sufficiently strong, the ring's expansion continues after breaching the flattened cloud. Nevertheless, Deharveng et al. (2010) claimed that a possible shortcoming of the scenario proposed by Beaumont & Williams (2010) is the absence of a bipolar nebula as a result of a double *champagne flow* effect along the poles of the IB (Tenorio Tagle et al. 1979).

4.3. Energetics of RCW 78 and MB

In our simple model, the main ionizing source of RCW 78 is the Lyman continuum flux of the WR star WR 55. The latter is also the driving source, via the mechanical energy injected by its stellar wind, of the expansion of the molecular gas associated with RCW 78. Is WR 55 capable of powering RCW 78 and providing the mechanical energy needed to power the expansion of the molecular gas?

To answer the first question, we have to calculate the number of Lyman continuum photons needed to keep the current level of ionization in RCW 78. To this end, the continuum flux densities of CF2, CF3, CF4, CF5, and CF6 were added up, and using Eq. (8) under the assumption that $T_{\text{e}} \approx 10^4 \text{ K}$ and $d \approx 5 \text{ kpc}$, we derived $N_{\nu} \approx 1 \times 10^{48} \text{ s}^{-1}$. Assuming that the number of Lyman continuum photons emitted by a WN7 star is $\sim 2.5 \times 10^{49} \text{ s}^{-1}$ (Crowther 2007), the WR star may be capable of maintaining the ionization level of RCW 78.

In relation to the point of whether the mechanical energy injected by WR 55 could be driving the expansion of MB, we derive a rough figure for the total mechanical energy injected via stellar winds by both WR 55 and its progenitor. The wind mechanical energy (E_{w}) is estimated to be

$$E_{\text{w}} = L_{\text{w}} t_{\text{w}} = \frac{1}{2} \dot{M} V_{\text{w}}^2 t_{\text{d}}, \quad (11)$$

where \dot{M} is the mass-loss rate in units of $M_{\odot} \text{ yr}^{-1}$, V_w is the wind terminal velocity in units of km s^{-1} , and t_d is the time spent by the star during either the WR or the main-sequence phase. Adopting for WR 55 a mass-loss rate $\dot{M} = 2 \times 10^{-5} M_{\odot} \text{ yr}^{-1}$, a terminal wind velocity $V_w = 1960 \text{ km s}^{-1}$ (Smith et al. 2002), and $t_{WN} \approx 5 \times 10^5 \text{ yr}$ (van der Hucht 2001), we derived a mechanical energy of $E_{WN} \approx 3.8 \times 10^{50} \text{ erg}$. Considering an O3V star as the progenitor of the WN star (Massey 1998), assuming $\dot{M} = 1.41 \times 10^{-6} M_{\odot} \text{ yr}^{-1}$ and $V_w = 3150 \text{ km s}^{-1}$ for this spectral type (Smith et al. 2002), and adopting a main-sequence lifetime of $t_0 \approx 2 \times 10^6 \text{ yr}$ (Massey 1998), the mechanical energy injected during the main sequence is $E_0 \approx 2.8 \times 10^{50} \text{ erg}$. Therefore, the total mechanical energy injected into the interstellar medium is $E_{\text{tot}} \approx 6.6 \times 10^{50} \text{ erg}$. Taking into account that the expanding kinetic energy of MB is $E_{\text{kin}} \sim 9 \times 10^{48} \text{ erg}$ (see Table 3), only about 1.4% of the mechanical energy released by WR 55 and its progenitor would be needed to account for the kinetic energy of the expanding molecular gas. This estimate is in good agreement with the conversion efficiencies of approximately 2–5% reported by H α line studies of IBs (Cappa et al. 1996; Cichowolski et al. 2001, 2003). Theoretical models also suggest that in adiabatic wind bubbles only a few percent of the injected mechanical energy will be converted into kinetic energy of the expanding gas (Weaver et al. 1977; Koo & McKee 1992; Arthur 2007). Based on the above consideration, the stellar winds of both WR 55 and its progenitor are able to provide the observed kinetic energy of MB. In relation to the momentum injected by the WR star and its progenitor to the ISM, we obtain $P_* \approx 2.1 \times 10^4 M_{\odot} \text{ km s}^{-1}$, which almost agrees with the momentum of MB (see Table 3). This indicates that the momentum is more tightly conserved in the system star-MB.

The dynamical age (yr) of a wind-blown bubble in the momentum-conserving case can be calculated using

$$t_d = 0.5 \times 10^6 \times \frac{R}{V_{\text{exp}}} \quad (12)$$

(McCrory 1983; Howarth & Lamers 1999), where R is the radius of the bubble (pc), and V_{exp} is the expansion velocity (km s^{-1}). Adopting $R \approx 13 \text{ pc}$ (linear length the semi-major axis) and $V_{\text{exp}} = 5 \text{ km s}^{-1}$, a value of $t_d \approx 1.3 \times 10^6 \text{ yr}$ is obtained for MB. Considering the uncertainties, this value agrees almost with the duration of the combined O and WN phases.

We note that the small solid angle ($\ll 4\pi$) subtended by MB reduces the wind mechanical energy and the ionizing power of WR 55 available to it. This may also help us to explain the tightness in the energy requirements (radiative and mechanical) and the dynamical age obtained before.

5. Summary

We have analyzed the ^{12}CO (1–0) and radio continuum emission distribution within a square region $25' \times 25'$ in size centered on the WN7 star HD 117688 (WR 55) around the optical nebula RCW 78 using intermediate angular-resolution CO data, high angular-resolution radio-continuum data at 1.4 GHz and 4.85 GHz, and H α data.

The CO data have allowed us to identify a molecular feature that is likely to be associated with RCW 78. This gas has a mean velocity of -49.5 km s^{-1} and its spatial distribution shows an excellent morphological correlation with the optical nebula. We have found that this feature is far from being homogeneous and have identified five molecular concentrations. Each one of them is very well-correlated with different areas of RCW 78. These molecular concentrations exhibit a clear radial velocity gradient.

The mean radial velocity of the different molecular concentrations and the radial velocity gradient measured for the CO is in good agreement with the H α data. The molecular gas related to RCW 78 has a total mass of $\sim 3.4 \times 10^4 M_{\odot}$.

High resolution continuum data have revealed the presence of six features towards RCW 78. Five of them, which have been denoted as CF2, CF3, CF4, CF5, and CF6, are likely to be associated with the nebula. Based on radio-continuum flux-density determinations at 1.4 GHz and 4.85 GHz all these sources are thermal in nature. A sixth radio continuum feature (labelled CF1) is also thermal and very likely related to HD 117797. Owing to the uncertainty in the distances of both HD 117797 and WR 55 (the WR star is associated with RCW 78), it is unclear whether both objects are related to each other, or HD 117797 is a foreground object to RCW 78.

A very simple model was developed to explain the radial velocity gradient depicted by the molecular gas, and some of the morphological properties measured for RCW 78. The model consists of an expanding ring-like structure of molecular gas, whose inner face is being ionized by the Lyman continuum photons emitted by WR 55. The ring-like feature is inclined by $\sim 60^\circ$ with respect to the sky plane, and has a low expansion velocity of $\sim 5 \text{ km s}^{-1}$. The WR star may well be the main ionization source of the nebula RCW 78 and the driving source of the expansion of the associated molecular gas.

Acknowledgements. We acknowledge the referee, Prof. You-Hua Chu, and the editor, Malcolm Walmsley for their helpful comments and suggestions that improved the presentation of this paper. N.U.D. is grateful to Prof. Serge Pineault for his helpful suggestions at early stages of this work. This project was partially financed by the Consejo Nacional de Investigaciones Científicas y Técnicas (CONICET) of Argentina under projects PIP 112-200801-01299, Universidad Nacional de La Plata (UNLP) under project 11G/091, and Agencia Nacional de Promoción Científica y Tecnológica (ANPCYT) under project PICT 14018/03. This research has made use of the VIZIER database, operated at the CDS, Strasbourg, France. We greatly appreciate the hospitality of all staff members of Las Campanas Observatory of the Carnegie Institute of Washington. We thank all members of the NANTEN staff, in particular Prof. Yasuo Fukui, Dr. Toshikazu Onishi, Dr. Akira Mizuno, and students Y. Moriguchi, H. Saito, and S. Sakamoto. We also would like to thank Dr. D. Miniti (Pontificia Universidad Católica, Chile) and Mr. F. Bareilles (IAR) for their involvement in early stages of this project.

References

- Arnal, E. M. 1992, A&A, 254, 305
- Arnal, E. M., & Cappa, C. E. 1996, MNRAS, 279, 788
- Arnal, E. M., Cappa, C. E., Rizzo, J. R., & Cichowolski, S. 1999, AJ, 118, 1798
- Arthur, S. J. 2007, Wind-Blown Bubbles around Evolved Stars, ed. T. W. Hartquist, J. M. Pittard, & S. A. E. G. Falle, 183
- Beaumont, C. N., & Williams, J. P. 2010, ApJ, 709, 791
- Bohlin, R. C., Savage, B. D., & Drake, J. F. 1978, ApJ, 224, 132
- Brand, J., & Blitz, L. 1993, A&A, 275, 67
- Burton, W. B., & Gordon, M. A. 1978, A&A, 63, 7
- Cappa, C. E., Niemela, V. S., Herbstmeier, U., & Koribalski, B. 1996, A&A, 312, 283
- Cappa, C. E., Rubio, M., & Goss, W. M. 2001, AJ, 121, 2664
- Cappa, C. E., Rubio, M., Martín, M. C., & Romero, G. A. 2009, A&A, 508, 759
- Carey, S. J., Noriega-Crespo, A., Price, S. D., et al. 2005, in BAAS, 37, AAS Meeting Abstracts, 1252
- Castor, J., McCrary, R., & Weaver, R. 1975, ApJ, 200, L107
- Chaisson, E. J. 1976, in Frontiers of Astrophysics, ed. E. H. Avrett, 259
- Chu, Y.-H. 1981, ApJ, 249, 195
- Chu, Y.-H., & Treffers, R. R. 1981, ApJ, 250, 615
- Cichowolski, S., Pineault, S., Arnal, E. M., et al. 2001, AJ, 122, 1938
- Cichowolski, S., Arnal, E. M., Cappa, C. E., Pineault, S., & St-Louis, N. 2003, MNRAS, 343, 47
- Condon, J. J., Griffith, M. R., & Wright, A. E. 1993, AJ, 106, 1095
- Conti, P. S., & Vacca, W. D. 1990, AJ, 100, 431
- Crowther, P. A. 2007, ARA&A, 45, 177
- Deharveng, L., Schuller, F., Anderson, L. D., et al. 2010, A&A, 523, A6
- Dias, W. S., Alessi, B. S., Moitinho, A., & Lepine, J. R. D. 2010, VizieR Online Data Catalog, 10, 2022

- Dickman, R. L. 1978, ApJS, 37, 407
- Digel, S. W., Grenier, I. A., Heithausen, A., Hunter, S. D., & Thaddeus, P. 1996, ApJ, 463, 609
- Dyson, J. E. 1977, A&A, 59, 161
- Esteban, C. 1993, PASP, 105, 320
- Esteban, C., Vilchez, J. M., Manchado, A., & Edmunds, M. G. 1990, A&A, 227, 515
- Garcia-Segura, G., & Mac Low, M.-M. 1995, ApJ, 455, 145
- Georgelin, Y. M., Boulesteix, J., Georgelin, Y. P., Le Coarer, E., & Marcellin, M. 1988, A&A, 205, 95
- Haslam, C. G. T. 1974, A&AS, 15, 333
- Haverkorn, M., Gaensler, B. M., McClure-Griffiths, N. M., Dickey, J. M., & Green, A. J. 2006, ApJS, 167, 230
- Howarth, I., & Lamers, H. J. G. 1999, J. British Astron. Assoc., 109, 347
- Inoue, A. K. 2001, AJ, 122, 1788
- Koo, B.-C., & McKee, C. F. 1992, ApJ, 388, 93
- Kutner, M. L., & Ulrich, B. L. 1981, ApJ, 250, 341
- Marston, A. P. 2001, ApJ, 563, 875
- Martins, F., Schaerer, D., & Hillier, D. J. 2005, A&A, 436, 1049
- Massey, P. 1998, in The Stellar Initial Mass Function, 38th Herstmonceux Conference, ed. G. Gilmore, & D. Howell, ASP Conf. Ser., 142, 17
- McCray, R. 1983, Highlights of Astronomy, 6, 565
- Moriguchi, Y., Yamaguchi, N., Onishi, T., Mizuno, A., & Fukui, Y. 2001, PASJ, 53, 1025
- Parker, Q. A., Phillipps, S., Pierce, M. J., et al. 2005, MNRAS, 362, 689
- Penzias, A. A., & Burrus, C. A. 1973, ARA&A, 11, 51
- Rizzo, J. R., Martín-Pintado, J., & Henkel, C. 2001a, ApJ, 553, L181
- Rizzo, J. R., Martín-Pintado, J., & Mangum, J. G. 2001b, A&A, 366, 146
- Rodgers, A. W., Campbell, C. T., & Whiteoak, J. B. 1960, MNRAS, 121, 103
- Smith, L. J., Norris, R. P. F., & Crowther, P. A. 2002, MNRAS, 337, 1309
- Strong, A. W., & Mattox, J. R. 1996, A&A, 308, L21
- Tenorio Tagle, G., Yorke, H. W., & Bodenheimer, P. 1979, A&A, 80, 110
- Turner, D. G., & Forbes, D. 2005, PASP, 117, 967
- Ulrich, B. L., & Haas, R. W. 1976, ApJS, 30, 247
- van der Hucht, K. A. 2001, New A Rev., 45, 135
- Vasquez, J., Cappa, C., & McClure-Griffiths, N. M. 2005, MNRAS, 362, 681
- Vasquez, J., Cappa, C. E., & Pineault, S. 2009, MNRAS, 395, 2045
- Walborn, N. R. 1972, AJ, 77, 312
- Walborn, N. R. 1982, AJ, 87, 1300
- Weaver, R., McCray, R., Castor, J., Shapiro, P., & Moore, R. 1977, ApJ, 218, 377
- Yamaguchi, N., Mizuno, N., Saito, H., et al. 1999, PASJ, 51, 775